caspase 9 and then caspase 3.[3] However, activation of caspase 8 upstream of caspase 3 has also been demonstrated.[6]

Human mitochondrial DNA (mtDNA) is a circular DNA with 16,569 bp that encodes 13 subunits of complexes I, III, IV, and V of oxidative phosphorylation.[7] Although it has been shown that CDDP can cause mtDNA damage,[8] the role of mtDNA in CDDP-induced apoptosis is not clear. In this study, we compared cell survival, extent of apoptosis, activation of caspase 3, and cytochrome *c* release in 143B and 143B-$\rho^0$ cells following CDDP treatment.

## MATERIALS AND METHODS

The human osteosarcoma cell line, 143B cells (thymidine kinase deficient, TK), and 143B-$\rho^0$ cells (clone 143B-87) lacking mtDNA were obtained from Dr. Douglas Wallace at the University California, Irvine, CA.[9,10] The absence of mitochondrial gene expression has also been previously confirmed.[11] Both cell lines were cultured in high-glucose (4.5 g/L) Dulbecco's modified Eagle's medium supplemented with 10% fetal bovine serum, 110 μg/mL pyruvate, and 50 μg/mL uridine.

### *Evaluation of Cell Survival following CDDP Treatment*

The colony formation assay was used to test the clonogenic ability of cells. Approximately 200 cells were plated on 60-mm dishes for 24 h and exposed to various doses of CDDP for another 24 h.The number of visible colonies grown from single cells was counted after staining cells with crystal violet to evaluate cell survival following CDDP treatment.[12] The threshold to define a colony was set at 50 cells per colony, which was much less than the number of cells in regular colonies of control dishes.

### *Detection of Apoptosis-Associated Nucleosomal Ladder*

Total genomic DNA was isolated from cells using the Puregene DNA Isolation Kits from Gentra Systems (Minneapolis, MN). The ApoAlert ligation-mediated (LM)–PCR Ladder Assay kit from BD Biosciences Clontech (Palo Alto, CA) was used to determine the presence of nucleosomal ladder. The PCR products were electrophoresed in a 1.5% agarose gel containing ethidium bromide.

### *Measurement of Caspase 3 Activity*

The ApoAlert Caspase Fluorescent Assay kit from BD Biosciences Clontech was used. A total of $10^6$ cells were harvested, and supernatant from lysed cells was incubated with the substrate, DEVD-AFC (7-amino-4-trifluoromethyl coumarin), for 1 h at 37°C. Cleavage of the substrate by active caspase 3 resulted in the increase of fluorescence (excitation = 400 nm and emission = 505 nm), which was recorded by a 96-well fluorometer. The reading from no-substrate control was subtracted.

### *Western Blot Analysis for Detecting Cytochrome* c *Release*

Cells were homogenized in mitochondrial isolation solution (0.225 M mannitol, 0.075 M sucrose, 1 mM EGTA, pH 7.4) containing the protease inhibitor cocktail

from Roche (Mannheim, Germany) and centrifuged at 600 × *g*. The supernatant was centrifuged at 10,000 × *g*, and the final supernatant was the cytosolic fraction without nuclear and mitochondrial fractions. The final pellet was washed and resuspended in 50 mM potassium phosphate buffer (pH 7.4) containing 0.5% Triton X-100 and saved as the mitochondrial fraction. Proteins were size-separated by SDS–polyacrylamide gel electrophoresis and analyzed for cytochrome *c*, actin, and Mn superoxide dismutase (MnSOD) using antibodies obtained from BD Pharmingen (San Diego, CA), Chemicon (Temecula, CA), and Upstate (Charlottesville, VA), respectively.

### *Statistical Analysis*

Analysis of variance (ANOVA) was used to compare the difference among multiple groups using SASfor Windows version 8.1 (SAS Institute, Cary, NC). Data are presented as mean ± standard deviation.

## RESULTS AND DISCUSSION

Results of cell survival assay are shown in FIGURE 1. The doses of drug that inhibited 50% and 90% of colony formation, $IC_{50}$ and $IC_{90}$, were calculated from three independent experiments.[12] The $IC_{50}$ for 143B and 143B-$\rho^0$ cells was 0.37 ± 0.01 and 0.24 ± 0.01 μg/mL, respectively; and the $IC_{90}$ for 143B cells and 143B-$\rho^0$ cells was 0.77 ± 0.12 and 0.42 ± 0.03 μg/mL, respectively. Those results indicated that CDDP resulted in much lower cell survival in 143B-$\rho^0$ than in 143B cells, which could be caused by enhanced apoptosis or necrosis.

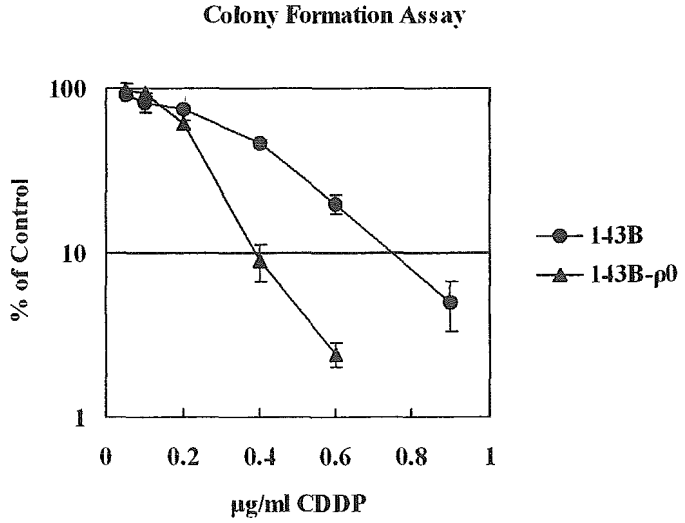


**FIGURE 1.** Cell survival curve following CDDP treatment obtained from colony formation assay. There are three dishes per group. The y-axis is in log scale.

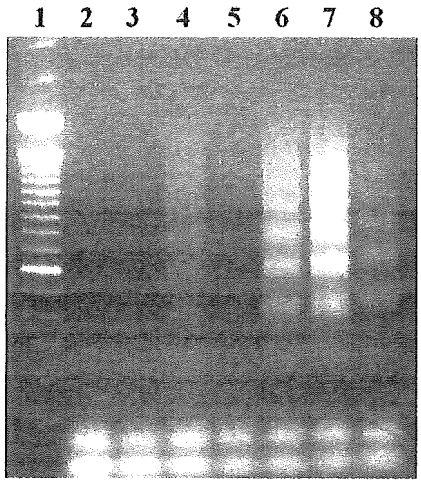


**FIGURE 2.** Detection of nucleosomal DNA ladder by LM-PCR. Lanes 1, 100-bp ladder; 2, 134B-control; 3, 143B-0.5 μg/mL CDDP; 4, 143B-1 μg/mL CDDP; 5, $\rho^0$-control; 6, $\rho^0$-0.5 μg/mL; 7, $\rho^0$-1 μg/mL; 8, positive control (calf thymus DNA).

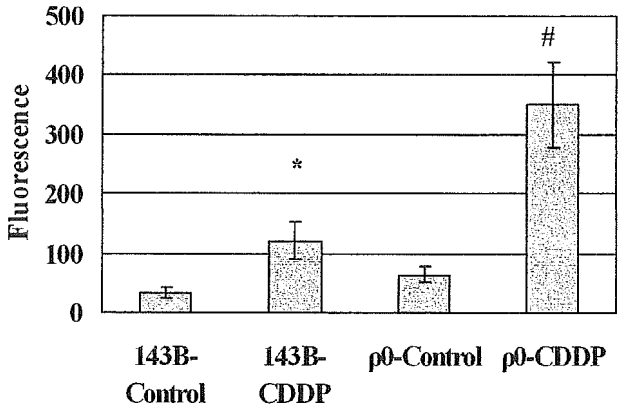


**FIGURE 3.** Caspase 3 activities following 24-h CDDP treatment (0.5 μg/mL). $^*P = .01$ for 143B-control versus 143B-CDDP; $^{\#}P < 0.0001$ for $\rho^0$-control versus $\rho^0$-CDDP. There are four replicates for each group.

We next investigated the effect of CDDP on apoptosis in these two cell lines. Results of LM-PCR (FIG. 2) demonstrated that 24-h CDDP treatment (0.5 and 1 μg/mL) induced a greater extent of apoptosis-associated DNA fragmentation in 143B-$\rho^0$ cells. Moreover, FIGURE 3 shows that 24-h CDDP treatment (0.5 μg/mL) increased caspase 3 activities in both cells. Two-way ANOVA revealed that the increase in 143B-$\rho^0$ cells was greater ($P = 0.0003$). Therefore, enhancement of CDDP-induced cell death by depletion of mtDNA was correlated with the increase in DNA fragmentation and caspase 3 activation.

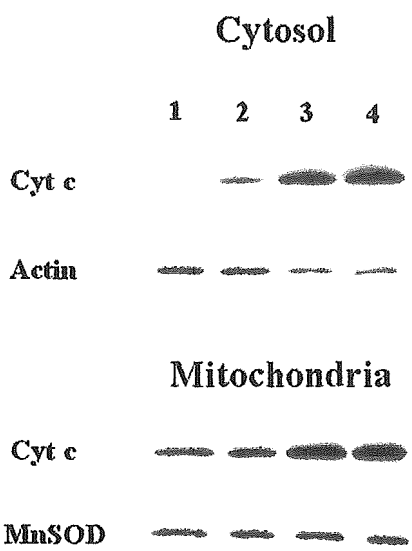


**FIGURE 4.** Western blot analysis for detection of cytochrome c release. Lanes 1, 2, 3, and 4 represent 143B-control, 143B-CDDP, $\rho^0$-control, and $\rho^0$-CDDP, respectively.

Furthermore, results of Western blot analysis (FIG. 4) showed that the amount of cytochrome c released into cytosol, relative to that of actin, was markedly increased by 24-h CDDP treatment (0.5 μg/mL) in 143B cells. The level of cytochrome *c* in cytosol was significantly higher in the control of 143B-$\rho^0$ cells than in 143B cells, although the increase after CDDP treatment was less obvious in 143B-$\rho^0$ cells. That could be due to the status of mitochondrial injury or a compensatory increase in cytochrome *c* expression because its level in mitochondria was also augmented in 143B-$\rho^0$ cells compared with that of MnSOD (FIG. 4). However, this increase did not lead to a proportional increase in the basal caspase 3 activity (FIG. 3), suggesting that 143B-$\rho^0$ cells could have become less sensitive to the death signal of cytochrome *c*, such as by suppression of apoptosome formation and caspase 9 activation,[5] during the stage without apoptotic insult. Persistent presence of higher levels of cytosolic cytochrome *c* in 143B-$\rho^0$ cells could result in greater caspase 3 activation by CDDP (FIG. 3), although cytochrome *c*–independent pathways might be also involved.

It has been shown that apoptosis and cytochrome *c* release induced by staurosporine were not altered following mtDNA depletion, demonstrating that those pathways were not impaired in $\rho^0$ cells.[10,13] However, apoptosis and translocation of cytochrome *c* were suppressed in $\rho^0$ cells after the treatment of tumor necrosis factor-related apoptosis–induced ligand (TRAIL),[14] whereas mtDNA depletion enhanced CDDP-induced apoptosis as shown by this study. Therefore, the use of $\rho^0$ cells has revealed diverse roles of mtDNA in apoptosis depending on the apoptotic stimuli used. Liang and Ullyatt also showed that CDDP-induced apoptosis was increased in $\rho^0$ cells derived from a lymphoma cell line (U937 cells) that was assessed by morphological changes, but they did not investigate any related apoptotic pathways.[15]

Our results first indicate that enhanced caspase 3 activation plays an important role in increased CDDP-induced cell death in 143B-$\rho^0$ cells. A higher degree of cytochrome *c* release in 143B-$\rho^0$ cells before treatment may be an important role, but mechanisms independent of cytochrome *c* release could be also enhanced, such as augmented activation of caspase 8 and release of Smac/DIABLO protein from mitochondria. Other mechanisms related to cytochrome *c*, such as the formation of apoptosome with apoptotic protease activating factor 1 (Apaf-1) and nitrosylation of cytochrome *c*, could be also important.[5,16] On the other hand, the existence of caspase-independent pathways in CDDP-induced apoptosis has been indicated.[17] Therefore, the role of caspase-independent mechanisms, such as release of apoptosis-inducing factor (AIF) from mitochondria, remains to be elucidated.[5] Furthermore, because mitochondrial dysfunction is known to induce oxidative stress and alter expression of nuclear genes,[7] chronic perturbation of redox status may result in different signaling pathways of cell death in response to CDDP in $\rho^0$ cells because CDDP can also increase oxidative stress.[1,2] However, as shown by this study, it is clear that the caspase-dependent pathway is, at least, a mechanism leading to increased extent of apoptosis by CDDP following mtDNA depletion in 143B cells.

## ACKNOWLEDGMENTS

This work is supported by Grant CMRP1230 from Chang Gung Memorial Hospital, Taiwan.

## REFERENCES

1. SIDDK, Z.H. 2003. Cisplatin: mode of cytotoxic action and molecular basis of resistance. Oncogene **22:** 7265–7279.
2. BAEK, S.M., C.H. KWON, J.H. KIM, *et al.* 2003. Differential roles of hydrogen peroxide and hydroxyl radical in cisplatin-induced cell death in renal proximal tubular epithelial cells. J. Lab. Clin. Med. **142:** 178–186.
3. MUELLER, T., W. VOIGT, H. SIMON, *et al.* 2003. Failure of activation of caspase-9 induces a higher threshold for apoptosis and cisplatin resistance in testicular cancer. Cancer Res. **63:** 513–522.
4. BURGER, H., K. NOOTER, A.W. BOERSMA, *et al.* 1997. Lack of correlation between cisplatin-induced apoptosis, p53 status and expression of Bcl-2 family proteins in testicular germ cell tumor cell lines. Int. J. Cancer **73:** 592–599.
5. HENGARTNER, M.O. 2000. The biochemistry of apoptosis. Nature **407:** 770–776.
6. HOTTA, T., H. SUZUKI, S. NAGAI, *et al.* 2003. Chemotherapeutic agents sensitize sarcoma cell lines to tumor necrosis factor-related apoptosis-inducing ligand-induced casepase-8 activation, apoptosis and loss of mitochondrial membrane potential. J. Orthop. Res. **21:** 949–957.
7. WALLACE, D.C. 1999. Mitochondrial diseases in man and mouse. Science **283:** 1482–1488.
8. OLIVERO, O.A., P.K. CHANG, D.M. LOPEZ-LARRAZA, *et al.* 1997. Preferential formation and decreased removal of cisplatin-DNA adducts in Chinese hamster ovary cell mitochondrial DNA as compared to nuclear DNA. Mutat. Res. **391:** 79–86.
9. TROUNCE, I., S. NEILL & D.C. WALLACE. 1994. Cytoplasmic transfer of the mtDNA nt 8993 T→G (ATP6) point mutation associated with Leigh syndrome into mtDNA-less cells demonstrates cosegregation with a decrease in state III respiration and ADP/O ratio. Proc. Natl. Acad. Sci. USA **91:** 8334–8338.
10. JIANG, S., J. CAI, D.C. WALLACE & D.P. JONES. 1999. Cytochrome c-mediated apoptosis in cells lacking mitochondrial DNA. J. Biol. Chem. **274:** 29905–29911.

11. YEN, H.C., C.Y. NIEN, H.J. MAJIMA, *et al.* 2003. Increase of lipid peroxidation by cisplatin in WI38 cells but not in SV40-transformed WI38 cells. J. Biochem. Mol. Toxicol. **17:** 39–46.
12. FRESHNEY, R.I. 2000. Culture of Animal Cells. A Manual of Basic Technique. 4th edit. John Wiley & Sons. New York.
13. CAI, J., D.C. WALLACE, B. ZHIVOTOVSKY & D.P. JONES. 2000. Separation of cytochrome c-dependent caspase activation from thiol-disulfide redox change in cells lacking mitochondrial DNA. Free Radic. Biol. Med. **29:** 334–342.
14. KIM, J., Y.H. KIM, Y. CHANG, *et al.* 2002. Resistance of mitochondrial DNA-deficient cells to TRAIL: role of Bax in TRAIL-induced apoptosis. Oncogene **21:** 3139–3148.
15. LIANG, B.C. & E. ULLYATT. 1998. Increased sensitivity to cis-diamminedichloroplatinum induced apoptosis with mitochondrial DNA depletion. Cell Death Differ. **5:** 694–701.
16. SCHONHOFF, C.M., B. GASTON & J.B. MANNICK. 2003. Nitrosylation of cytochrome c during apoptosis. J. Biol. Chem. **278:** 18265–18270.
17. HENKELS, K.M. & J.J. TURCHI. 1999. Cisplatin-induced apoptosis proceeds by caspase-3-dependent and -independent pathways in cisplatin-resistant and -sensitive human ovarian cancer cell lines. Cancer Res. **59:** 3077–3083.

Available online at www.sciencedirect.com

SCIENCE DIRECT®

Free Radical Biology & Medicine 38 (2005) 950–959

www.elsevier.com/locate/freeradbiomed

Original Contribution

# Levels of reactive oxygen species and primary antioxidant enzymes in WI38 versus transformed WI38 cells following bleomcyin treatment

Hsiu-Chuan Yen[a,*], Hui-Ming Chang[a], Hideyuki J. Majima[b], Fan-Yi Chen[a], Sin-Hua Li[a]

[a]*Graduate Institute of Medical Biotechnology and Department of Medical Biotechnology and Laboratory Science, Chang Gung University, Tao-Yuan 333, Taiwan*

[b]*Department of Oncology, Kagoshima University Graduate School of Medical and Dental Sciences, Kagoshima, Japan*

Received 29 July 2004; revised 30 November 2004; accepted 15 December 2004
Available online 11 January 2005

**Abstract**

Bleomycin (BLM) is an anticancer drug that generates reactive oxygen species (ROS) after interacting with iron and oxygen. We hypothesized that BLM could cause a different status of oxidative stress in normal versus tumor cells due to possible altered redox status and gene expression in cells following transformation. In this study, the extent of cytotoxicity, levels of ROS, and activities of antioxidant enzymes were compared between normal WI38 cells and SV40-transformed WI38 (VA13) cells following BLM treatment. Basal activities of MnSOD and catalase were lower in VA13 cells and basal ROS levels were higher in VA13 cells. Although BLM caused greater growth inhibition and apoptosis in VA13 cells, it increased ROS levels at an earlier time point in WI38 cells. Moreover, BLM treatment (100 μg/ml) had no effect on the activities of MnSOD, CuZnSOD, and catalase, but increased the activities of glutathione peroxidase (GPX) in WI38 cells after a 48-h treatment and in VA13 cells after a 24- and 48-h treatment. Northern blot analysis indicated that the increase in GPX activities was due to increased transcript levels of GPX1 but not GPX4 in both cells. Our results indicate selective induction of the GPX1 gene by BLM and different redox responses to BLM between WI38 and VA13 cells.


*Keywords:* Bleomycin; Reactive oxygen species; Antioxidant enzymes; Glutathione peroxidase; Transformed cells; Free radicals

## Introduction

Bleomycin (BLM) is a family of glycopeptidic antibiotics that is used as an anticancer drug in clinical use but it can also cause irreversible pulmonary toxicity in humans. BLM can interact with iron ions using five of its nitrogen atoms and bind to DNA with its bithiazole ring [1]. Based on experiments performed in test tubes, it has been postulated that after binding to Fe(II), BLM further complexes with molecular oxygen and generates the "activated BLM," possibly $HO_2$–Fe(III)-BLM, following subsequent reduction [2]. The activated BLM complex causes DNA strand breaksby abstraction of hydrogen from the C-4 position of the deoxyribose moiety [1]. During these reactions, superoxide and hydroxyl radicals are generated [2,3]. The Fe(III)-BLM complex would exert the same effect if reducing agents or enzymes are present [1,2,4,5]. The hydroxyl radicals produced can also lead to DNA strand breaks [3,5]. Superoxide and hydrogen peroxide may reactivate BLM for damaging DNA [2,3]. On the other hand, Kanofsky showed that the Fe(III)-BLM complex catalyzed the decomposition of long-chain unsaturated fatty acids with concurrent generation of singlet oxygen [6]. Not only the generation of ROS has been detected by electron spin resonance in vitro [2,3], but also formation of oxidative DNA adducts has been detected when directly exposing

*Abbreviations:* BLM, bleomycin; CAT, catalase; DIG, digoxigenin; DHR, dihydrorhodamine 123; GSH, glutathione; GPX, glutathione peroxidase; LM-PCR, ligation-mediated polymerase chain reaction; MDA, malondialdehyde; MEM, minimum essential media; NAC, *N*-acetyl-L-cysteine; NBT, nitroblue tetrazolium; ROS, reactive oxygen species; SOD, superoxide dismutase; TBARS, thiobarbituric acid-reactive substance.

* Corresponding author. Graduate Institute of Medical Biotechnology, Chang Gung University, 259-Wen-Hwa 1st Road, Kwei-Shan, Tao-Yuan 333, Taiwan. Fax: +886 3 2118692.

*E-mail address:* yen@mail.cgu.edu.tw (H.-C. Yen).

0891-5849/$ - see front matter © 2004 Elsevier Inc. All rights reserved.
doi:10.1016/j.freeradbiomed.2004.12.022

BLM to pure DNA [7] or erythrocyte suspensions [8]. Exposure of BLM to lymphocytes and thymocytes resulted in both single and double DNA strand breaks and apoptosis [9]. However, there was no direct evidence that ROS formation was increased by BLM in live cultured cells or in vivo. Moreover, it has been indicated that lipid peroxidation was enhanced by BLM because thiobarbituric acid-reactive substance (TBARS) for the measurement of malondialdehyde (MDA) was increased in cultured cells or animal lungs after BLM treatment [10,11], but it is now known that TBARS is not a reliable marker of lipid peroxidation [12] and MDA could be produced from the base propenal from BLM-degraded DNA [5,13].

Superoxide dismutase (SOD), catalase (CAT), and glutathione peroxidase (GPX) are the primary antioxidant enzymes that can directly scavenge ROS. SOD catalyzes the dismutation of superoxide radicals to hydrogen peroxide and oxygen. Hydrogen peroxide is further detoxified by CAT and GPX. Hydrogen peroxide and lipid hydroperoxide are reduced by GPX at the expense of glutathione (GSH) [14]. The SOD family consists of cytosolic CuZnSOD (SOD1), mitochondrial MnSOD (SOD2), and extracellular ECSOD (SOD3) [15]. Five different mammalian GPX enzymes have also been identified. GPX1 and GPX4 are ubiquitous in all types of cells and they are present in both cytosol and mitochondria, but only GPX4 can repair lipid hydroperoxide esterified on phospholipids [16,17]. Gene expression or activities of those antioxidant enzymes, especially MnSOD and GPX1, have been shown to be differentially modulated by a variety of stimuli, such as ionizing radiation, cytokines, and various oxidative insults [18–24]. On the other hand, expression of some of these antioxidant enzymes could be modulated by redox-sensitive transcription factors, such as AP-1 and NF-κB [25,26].

Previous studies investigating the effects of BLM on levels of antioxidant enzymes in animal lungs showed alteration of several antioxidant enzymes with inconsistent conclusions. Elevation of GPX activities in normal lungs at several days post-treatment has been observed [10,27–29], but it has also been found that BLM decreased GPX activity in cultured lung fibroblasts [30]. However, those previous studies only measured the total activities but not the mRNA levels of specific forms of enzymes. Also only the activities of total SOD, but not CuZnSOD and MnSOD individually, were measured in those experiments.

Differences in levels of ROS, activities of antioxidant enzymes, and responses to agents producing oxidative stress between normal and tumor cells have been implicated in the roles of oxidative stress in tumorogenesis and cancer treatment [31–35]. However, comparison of cellular or molecular changes related to oxidative stress or antioxidant enzymes using different sources of normal and tumor cells in many studies may lead to inconsistent conclusions due to intrinsic individual variations. The normal human embryonic lung fibroblast cells, WI38, and the SV40-transformed WI38 cell line, VA13 cells, were from the same origin and have been widely used to examine the effects of transformation on cellular changes and responses [31,35–39]. Oberley et al. showed that the activity of MnSOD and the level of immunoreactive MnSOD protein were lower in VA13 cells compared to WI38 cells [36]. Wan and coworkers found that total glutathione levels were much higher in VA13 cells and WI38 cells were more sensitive to cytotoxicity induced by L-buthionine sulfoximine, an agent that inhibits glutathione synthesis [37]. Allen and Balin showed that glutathione concentration was increased by increased ambient oxygen tension in WI38 cells but that in SV40-transformed WI38 cells failed to response to elevated oxygen tension, although the glutathione level was higher in transformed WI38 cells at lower oxygen tensions [31]. We have also previously shown that the anticancer drug cisplatin augmented lipid peroxidation in WI38 cell but not VA13 cells [35]. However, basal levels of ROS, GPX, and CAT and responses to BLM treatment have not been compared between these two cells.

Different redox status and other characteristics between normal and tumor cells could result in differential responses to agents inducing oxidative stress. It is therefore important to compare the effects of BLM on redox status between normal and transformed cells, which would provide more insights for improvement of cancer therapy using BLM. In this study, we examined the effects of BLM on cytotoxicity, the extent of apoptosis-associated DNA fragmentation, the levels of ROS, and the levels of primary antioxidant enzymes in WI38 and VA13 cells.

## Materials and methods

### *Cell culture*

The embryonic human lung fibroblast WI38 cell (ATCC CCL 75) and its SV40-transformed subline VA13 cell (ATCC CCL 75.1) were obtained from Riken Cell Bank, Japan. The passage number of WI38 cells used in this study was 28–34. Both cells were maintained in minimum essential media (MEM) with Earl's salts supplemented with 10% defined fetal bovine serum. Cells were cultured in a humidified atmosphere of 5% $CO_2$ and 95% air at 37°C.

### *Cytotoxicity assay*

The 15-mg potency of bleomycin hydrochloride in individual ampoules was purchased from Nippon Kayaku Co. (Tokyo, Japan). Cytotoxicity was evaluated by the inhibition of cell growth or reduction of cell viability. Cells grown in 96-well tissue culture plates were treated with various doses of BLM for 48 h and were incubated with the reagent in the CellTiter 96 AQueous One solution cell proliferation assay kit (Promega, WI). The absorbance of reduced tetrazolium compound derived from the reagent due to dehydrogenase activities in viable cells was recorded at

490 nm with the subtraction of absorbance of background at 650 nm. Furthermore, cell numbers in 6-well plates were also counted after a 24-or 48-h BLM treatment at a dose of 100 μg/ml.

*Ligation-mediated polymerase chain reaction (LM-PCR) for the detection of apoptosis-induced nucleosomal ladder*

Total genomic DNA was isolated from cells using the Puregene DNA isolation kits from Gentra Systems (Minneapolis, MN). The ApoAlert LM-PCR ladder assay kit from Clontech (Polo Alto, CA) and gel electrophoresis were used to analyze the extent of apoptosis-induced nucleosomal ladder following BLM treatment. LM-PCR was performed according to the manufacturer's instruction. In this study, 500 ng of DNA was used in the ligation reaction to ligate adaptors to the ends of DNA fragments. To further amplify the DNA fragments, 150 ng of ligated DNA was added into the PCR in which the 24-mer adaptor was used as primers and 22 PCR cycles were carried out. The PCR products were electrophoresed in 1.5% agarose gel containing ethidium bromide.

*Detection of ROS by dihydrorhodamine 123 (DHR) staining*

DHR is an uncharged and nonfluorescent dye that can passively diffuse across membranes. It can be oxidized by ROS to fluorescent and positively charged rhodamine 123, which is preferentially localized in mitochondria [40]. Quantification of ROS levels by the DHR reaction was performed following previous published methods [41,42]. In brief, monolayers of cells grown on glass-bottomed 35-mm dishes (MatTek Corp., Ashland, MA) were prepared. After treatment with BLM, cells were reacted with DHR (Molecular Probes, Eugene, OR) at 37°C for 15 min at a final concentration of 10 μg/ml in a modified Hanks' balanced salt solution (HBSS) containing 10 mM Hepes, 1 mM $MgCl_2$, 2 mM $CaCl_2$, and 2.7 mM glucose and washed with the same buffer twice. Images of rhodamine 123 florescence due to oxidation of DHR were acquired using a CSU-10 confocal laser scanning unit (Yokogawa Electric Co., Tokyo, Japan) coupled to an LX90 inverted microscope (Olympus Optical Co.) and a C5810-01 color chilled 3CCD camera (Hamamatsu Photonics K.K., Japan). Rhodamine 123 from DHR was excited at 488 nm and emission was filtered using a 515-nm barrier filter. Several fields of cells in one dish were scanned randomly and images were recorded. Fluorescent intensity per unit area of each field was quantified using IPLab Spectrum version 3.0 software (Scanalytics Inc., Fairfax, VA). The mean of fluorescent intensity in arbitrary units from several areas in each acquired field was obtained.

*SOD activity assay*

SOD activity assay was performed according to the method of Spitz and Oberley [43]. Cells were homogenized in 50 mM potassium phosphate buffer (pH 7.8). Total SOD activity was assayed at 25°C by the nitroblue tetrazolium (NBT) reduction assay with bathocuproine sulfonate. The rate of reduction of NBT by superoxide, which was generated from xanthine and xanthine oxidase, was monitored spectrophotometrically at 560 nm. One unit of SOD was defined as the amount of protein which causes a 50% inhibition of the rate of NBT reduction. Sodium cyanide at the concentration of 5 mM was included in the assay mixture to measure MnSOD activity by inhibiting CuZn-SOD. CuZnSOD activity was the difference between total SOD activity and MnSOD activity.

*CAT activity assay*

CAT activity was measured by the method of Beers and Sizer with slight modifications [44]. For both CAT and GPX activity assays, same preparation of samples was used by homogenizing cells in 50 mM phosphate buffer (pH 7.4). Supernatant from 1000*g* centrifugation of cell homogenates was used for assays. The assay reaction for CAT consisted of 50 mM potassium phosphate buffer (pH 7.0), 0.02 M $H_2O_2$, and samples in a total volume of 1 ml. The reaction was carried out at 25°C. The rate of absorbance change ($\Delta A$/min) at 240 nm was recorded, which indicated the decomposition of $H_2O_2$. Activities were calculated using the molar extinction coefficient of $H_2O_2$ at 240 nm, 43.59 L/mol-cm.

*GPX activity assay*

Activity assays of selenium-dependent GPX were performed as previously described [45,46]. The coupling reagent consisted of 50 mM Tris-Cl buffer (pH 7.7), glutathione, glutathione reductase, sodium cyanide, and NADPH. The coupling reagent in 875 μl and 100 μl of sample was incubated for 2 min at 25°C and hydrogen peroxide (final 25 μM) was added to initiate the reaction. $\Delta A$/min at 340 nm was recorded. $\Delta A$/min of blank, in which sample was replaced by Tris-Cl buffer, was also recorded. The net $\Delta A$/min of samples after subtracting the blank rate was used to calculate the GPX activity using the molar extinction coefficient of NADPH at 340 nm, 6220 L/mol-cm.

*Nonradioactive Northern blot analysis*

Total RNA was isolated by Trizol (Invitrogen, Carlsbad, CA). The concentration of RNA was determined by measuring the absorbance at 260 nm. Nonradioactive Northern blot analysis to detect steady-state levels of mRNA was performed according to our previous established methods [35]. In brief, 15 μg of total RNA was electrophoresed in 1.5% formaldehyde–agarose gel and transferred to the positive-charged nylon membranes (Roche, USA) in 10X SSC (3 M sodium chloride and 300 mM sodium citrate, pH 7.0 for 20X SSC). Digoxigenin (DIG)-labeled probes for

cDNA fragments of GPX1, GPX4, and MnSOD genes were generated by the PCR DIG probe synthesis kit (Roche) using plasmids containing partial cDNA of those genes as the templates. These plasmids were purified from bacterial clones purchased from Invitrogen except that for MnSOD, which was made in the previous study [39]. Primers for GPX1 were 5′TGACACCCGGCACTTATTAGTGG3′ and 5′GCTTATGACCGACCCCAAGCT3′. Primers for GPX4 were 5′GGCAAGACCGAACTAAACTAC3′ and 5′GTGCACGCTGGATTTTCGG3′. Primers for MnSOD were 5′AGAAGCACAGCCTCCCCGAC3′ and 5′GCAAGCCATGTATCTTTCAGTTA3′. Membranes were prehybridized in hydridization solution (50% deionized formamide, 5X SSC, 0.1% *N*-lauroylsarcosine, 0.02% SDS, 2% blocking reagent from Roche) at 42°C for 1 h and then hybridized with probes in hydridization solution at 42°C overnight. The membrane was then washed twice and detected by the DIG luminescent detection kit (Roche) with alkaline phosphatase-conjugated anti-DIG antibody according to the manufacturer's instruction. Chemiluminescent bands were detected by exposing membranes to the BioMax ML film (Kodak, Rochester, NY). The density of signals on the film from Northern blot analysis and of the 28S rRNA band on the RNA gels photographed by the ChemiDoc system (Biorad, Hercules, CA) was analyzed by the Quantity One Software (Biorad).

*Statistical analysis*

Data were analyzed by SAS Win 8.1 software (SAS Institute, Cary, NC). One-way analysis of variance (ANOVA) was used to compare the difference among multiple groups. Complete block design was used for data of antioxidant enzyme activities from more than one set of experiments. Data were presented as mean ± standard deviation (SD) except that mean ± standard error of mean (SE) was used for different sets of Northern blot analysis. A level of $P < 0.05$ was considered statistically significant for most experiments except for results of Northern blot analysis in which $P < 0.1$ was considered significant due to the semiquantitative features of Northern blot analysis.

## Results

*Inhibition of cell growth and Induction of apoptosis by BLM*

To compare the effect of 48-h BLM treatment on the cytotoxicity in WI38 and VA13 cells, the amount of viable cells remaining was first accessed by the colorimetric method over a range of doses (10–1000 μg/ml) of BLM and the exact cell number remaining after a 24-or 48-h BLM treatment was counted in both cells at a dose of 100 μg/ml. As shown by Fig. 1, BLM markedly inhibited more growth of viable cells in VA13 cells than in WI38 cells when compared to control groups. The doses that inhibited 50% of

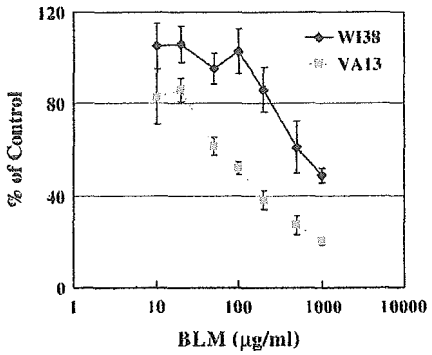


Fig. 1. Growth inhibition assay with a range of BLM doses using the colorimetric method following 48-h treatment. Amount of viable cells was detected by the colorimetric method. Data were represented as percentage of absorbance relative to mean of the control groups ($n = 3$ for each group). The $x$ axis is in log scale.

growth in WI38 and VA13 cells were approximately 120 and 950 μg/ml, respectively. By counting the cell number directly, we confirmed that there were significantly less VA13 cells remaining than WI38 cells following 100 μg/ml of BLM treatment for either 24 or 48 h (Fig. 2). The reduction in cell number was significant in WI38 cells only after a 48-h treatment but not after a 24-h treatment. The extent of reduction was also greater in VA13 cells than in WI38 cells. Most of the cells remaining could not be stained by trypan blue (data not shown). To further evaluate the role of apoptosis in the reduction of cell number after BLM treatment, LM-PCR was performed at different time points. Fig. 3 shows that both WI38 and VA13 cells had the greatest degree of apoptosis-associated nucleosomal fragmentation 24 h after BLM treatment. VA13 cells revealed a higher degree of apoptosis than WI38 cells overall.

*Levels of ROS*

To measure the production of ROS in cells, DHR was used as the indicator. Cells were treated with 100 μg/ml of CPT for 24 or 48 h and incubated with DHR. As shown in Table 1, there was a significant increase in fluorescent intensity of DHR in WI38 after a 24-h BLM treatment but not in VA13 cells. However, DHR-detectable ROS levels were significantly increased in both WI38 and VA13 cells after a 48-h BLM treatment. On the other hand, the basal level of DHR-detectable ROS was higher in VA13 controls than in WI38 controls. The images of increased fluorescence following 48-h BLM treatment in both cells are demonstrated in Fig. 4.

*Activities of primary antioxidant enzymes*

Tables 2 and 3 show the activities of primary antioxidant enzymes after 24-and 48-h BLM treatments, respectively. The data were combined from two sets of experiments and analyzed by the complete block design. BLM had no significant effect on the activities of MnSOD, CuZnSOD,

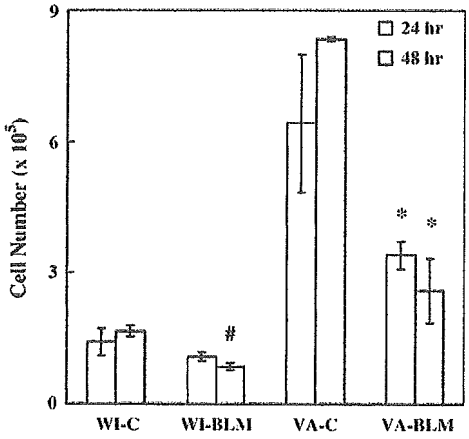


Fig. 2. Percentage of cell number remaining relative to control after 24-and 48-h BLM treatments. Numbers of cells were counted after 24- and 48-h BLM treatments at the dose of 100 μg/mg. Control cells were near confluence at the end of 48-h treatment. Cells remaining in treated groups were all significantly ($P < 0.05$) reduced compared to control groups except that in 24-h treated WI38 groups. WI, WI38 cells; VA, VA13 cells; C, control groups; BLM, BLM-treated groups; # significant difference from WI-C; * significant difference from VA-C.

and CAT. However, BLM increased GPX activities as early as 24 h after BLM treatment and the effect was still significant after a 48-h treatment in VA13 cells. The increase of GPX activity by BLM in WI38 cells was observed only after a 48-h treatment. Moreover, there was no difference in the basal activities of GPX between two cells but those of MnSOD and CAT were significantly lower in VA13 cells compared to WI38 cells.

*Steady-state mRNA levels of GPX1, GPX4, and MnSOD*

To elucidate whether the increase of GPX activities by BLM was due to up-regulation mRNA levels, we performed nonradioactive Northern blot analysis to detect steady-state

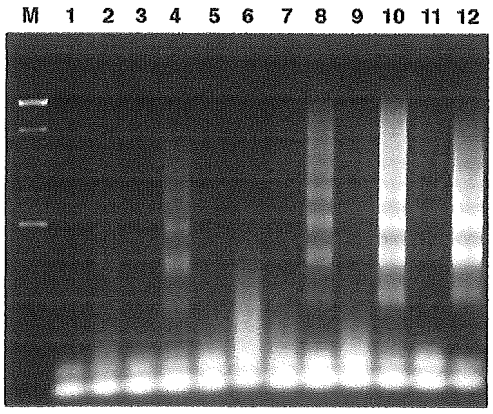


Fig. 3. Ligation-mediated PCR to detect apoptosis-associated DNA fragmentation. DNA was isolated from control cells and cells were treated with 100 μg/mg of BLM for various time points. M, 100-bp ladder; 1, 8-h WI-C; 2, 8-h WI-BLM; 3, 24-h WI-C; 4, 24-h WI-BLM; 5, 48-h WI-C; 6, 48-h WI-BLM; 7, 8-h VA-C; 8, 8-h VA-BLM; 9, 24-h VA-C; 10, 24-h VA-BLM; 11, 48-h VA-C; 12, 48-h VA-BLM.

Table 1
Quantification of intracellular ROS levels detected by DHR

| Group | Intensity (arbitrary units) | |
|---|---|---|
| | 24 h | 48 h |
| WI-control | 27.4 ± 1.4 (11) | 34.7 ± 1.3 (7) |
| WI-BLM | 31.0 ± 2.1 (10)[a] | 41.7 ± 2.5 (7)[a] |
| VA-control | 31.0 ± 2.7 (10)[b] | 40.2 ± 2.8 (7)[b] |
| VA-BLM | 32.6 ± 3.0 (10) | 55.8 ± 8.5 (6)[c] |

Data were presented as mean ± SD (number of replicates).
[a] Significant difference from WI38-control group.
[b] Significant difference from WI38-control group.
[c] Significant difference from VA13-control group.

mRNA levels of GPX1 and GPX4 in cells after BLM treatment (Fig. 5 and Fig. 6). The amount of 28S rRNA visualized on RNA gels was used to normalize the levels of transcripts on films because we have found that the levels of some frequently used housekeeping genes may not exactly match with that of RNA amounts on gels after treatment (data not shown). Fig. 5A and Fig. 5B show the representative results of RNA gels and transcript levels of GPX1 after 24-and 48-h treatments, respectively. The quality of RNA was excellent since the amount of 28S rRNA (upper bands) was much greater than that of 18S rRNA (lower bands). Fig. 5C shows the changes, calculated for three independent experiments, of each group relative to the control of WI38 cells (WI-C) for each time point and their statistical analysis. The results of Fig. 5 demonstrate that the mRNA level of GPX1 was significantly increased in VA13 cells after both a 24-and a 48-h treatment, while it was only increased in WI38 cells after 48 h. We considered $P < 0.1$ as a significant difference because the degrees of the increase in transcript levels could be very variable even though the trend of increase was consistent from experiment to experiment. On the other hand, the basal level of GPX1 between control groups of two cells was not different.

Because MnSOD is highly inducible and, as a mitochondrial matrix protein, its activity could be easily subjected to posttranslational controls by mitochondrial status [47], steady-state mRNA levels of MnSOD after 24-and 48-h BLM treatments were also investigated. Fig. 6 showed the results from one representative experiment examining mRNA levels of GPX4 and MnSOD from the same blot. Statistical analysis from three independent experiments indicated that GPX4 gene expression was not obviously altered by BLM treatment in both cells and was not different between two cells after normalized by the amount of 28S rRNA on gels (data not shown). Moreover, the basal transcript levels of GPX4 were not different between WI38 and VA13 cells. On the other hand, in agreement with the results of activity assays, mRNA levels of MnSOD were much higher in WI38 cells than in VA13 cells for both 1-and 4-kb transcripts, but not changed to a considerable amount after BLM treatment from two sets of experiments. The levels of the 1-kb transcript in the control of VA13 cells shown by Fig. 6 were about 60 and 50% of that in the

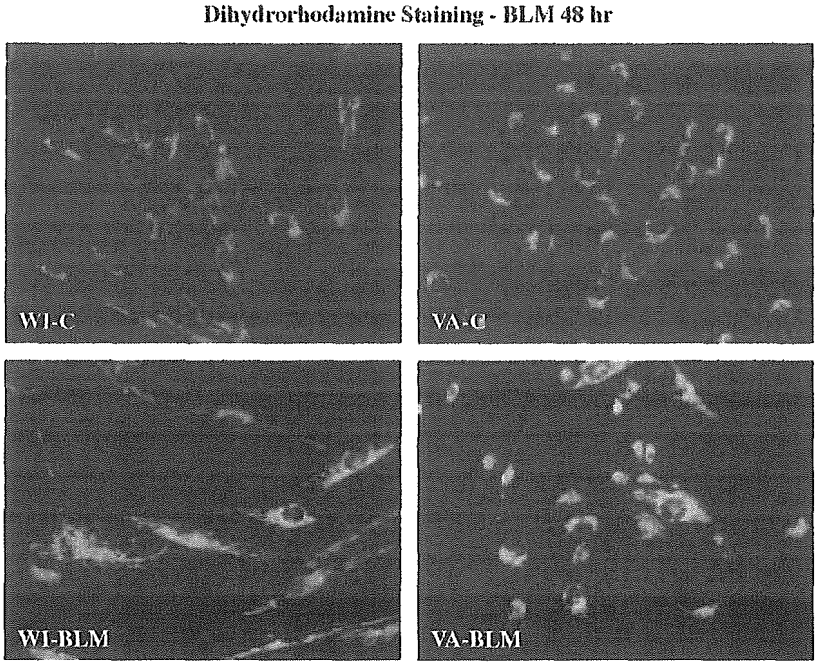


Fig. 4. Intracellular ROS detected by DHR after 48-h BLM treatment. The fluorescence intensity was significantly increased after BLM treatment in both cells.

control of WI38 cells for the 24-and 48-h treatment groups, respectively. However, the basal levels of the 4-kb transcript in VA cells were about 40 and 30% of those in WI38 cells for the 24-and 48-h treatment groups, respectively.

## Discussion

As an anticancer drug, BLM unsurprisingly caused a higher degree of growth inhibition and apoptosis in VA13 cells than normal WI38 cells. However, BLM induced oxidative stress earlier in WI38 cells than in VA13 cells as demonstrated by an earlier increase of DHR-detectable intracellular ROS levels and later induction of GPX1 in WI38 cells, which may not be directly linked to the DNA-damaging effect of BLM. Therefore, when normal WI38 cells became transformed, it presented a different status of oxidative stress in response to BLM.

No previous study demonstrated generation of intracellular ROS from BLM in live cultured cells or in animal tissues. DHR is a diffusible compound that is able to detect ROS such as hydrogen peroxide in the presence of peroxidases, hydroxyl radicals, and peroxynitrite, but not superoxide radicals [48,49]. Because oxidized DHR, rhodamine 123, is detected in the mitochondria, increased DHR oxidation may indicate ROS generation in mitochondria or in the compartments close to mitochondria. By using this method, we showed that BLM could increase intracellular ROS levels after both 24-and 48-h treatments in WI38 cells but only after a 48-h treatment in VA13 cells. However, we could not identify which species of ROS were generated.

The earlier increase of GPX activities in VA13 cells after BLM treatment could contribute to a lesser increase in DHR-detectable ROS levels in VA13 cells, which could be a response to BLM-generated oxidative stress but may not compensate for increased oxidative stress. However, the growth inhibitory effect of BLM was much greater to VA13 cells than to WI38 cells, which could result from preferential effects of DNA strand breaks and chromosomal aberrations induced by BLM [9] in fast-proliferating tumor cells. It is possible that formation of nuclear ROS is not readily detected by DHR or ROS formation was not the only

Table 2
Activities of primary antioxidant enzymes after 24-h BLM treatment

| | CuZnSOD (units/mg) | MnSOD (units/mg) | CAT (μmol/min/mg) | GPX (nmol/min/mg) |
|---|---|---|---|---|
| WI-control | 21.7 ± 5.0 (5) | 30.7 ± 5.3 (5) | 10.8 ± 2.8 (7) | 18.1 ± 2.5 (6) |
| WI-BLM | 23.5 ± 1.8 (4) | 28.8 ± 6.7 (4) | 10.0 ± 1.9 (7) | 16.7 ± 2.4 (6) |
| VA-control | 19.2 ± 2.0 (5) | 5.0 ± 1.9 (5)[a] | 6.6 ± 1.1 (6)[a] | 21.2 ± 5.1 (6) |
| VA-BLM | 19.6 ± 5.8 (4) | 4.8 ± 0.5 (4)[a] | 6.8 ± 1.4 (6)[a] | 27.7 ± 4.1 (6)[b] |

Data were presented as mean ± SD (number of replicates).
[a] Significant difference from WI38-control or WI38-BLM group.
[b] Significant difference from VA13-control group.

Table 3
Activities of primary antioxidant enzymes after 48-h BLM treatment

| | CuZnSOD (units/mg) | MnSOD (units/mg) | CAT (μmol/min/mg) | GPX (nmol/min/mg) |
|---|---|---|---|---|
| WI-control | 18.4 ± 8.6 (5) | 21.9 ± 13.0 (5) | 10.6 ± 2.4 (6) | 21.8 ± 5.2 (6) |
| WI-BLM | 20.5 ± 7.2 (5) | 29.4 ± 12.2 (5) | 9.9 ± 0.7 (6) | 37.5 ± 14.0 (6)[a] |
| VA-control | 17.2 ± 2.0 (5) | 4.2 ± 1.4 (5)[b] | 7.8 ± 1.4 (6)[b] | 20.7 ± 2.2 (6) |
| VA-BLM | 17.8 ± 3.8 (5) | 4.4 ± 1.3 (5)[b] | 5.9 ± 0.9 (6)[b] | 31.1 ± 3.5 (6)[c] |

Data were presented as mean ± SD (number of replicates).
[a] Significant difference from WI38-control group.
[b] Significant difference from WI38-control or WI38-BLM group.
[c] Significant difference from VA13-control group.

determinant in DNA damage following BLM treatment since some researchers proposed that BLM-induced strand break and base propenal formation could be independent from ROS [1,13]. It is also possible that lower basal activities of MnSOD and CAT in VA13 cells made VA13 cells more susceptible to oxidative damage and apoptosis by BLM. Moreover, ROS undetectable by DHR, such as superoxide, could be involved as MnSOD was able to protect cells against oxidative stress-associated apoptosis [41,50]. Nevertheless, earlier oxidative stress in WI38 cells would result in the interruption of normal cellular function, although there may be no immediate effect on growth. Furthermore, generation of ROS or oxidative damage induced by BLM in intact cells was not necessarily confined in the nuclei and therefore its possible adverse effects on other cellular compartments, such as mitochondria, and other macromolecules, such as lipid and protein, would have great implications in BLM-induced toxicity, which has not been well studied in the literature.

We have found that *N*-acetyl-L-cysteine (NAC) at 1 mM, which could completely protect VA13 cells against cytotoxicity induced by a 48-h treatment of hydrogen peroxide (100 μM) when treated together with hydrogen peroxide, was unable to exert any protective effect against BLM (500 μg/ml)-induced cytotoxicity in either WI38 or VA13 cells using the colorimetric assay either by pretreating cells with NAC before BLM treatment or by treating cells with NAC at the same time as BLM treatment (data not shown). NAC has been widely used an antioxidant that can both enhance intracellular GSH [51] and directly scavenge some species of ROS, especially hydroxyl radicals [52–54]. It has been

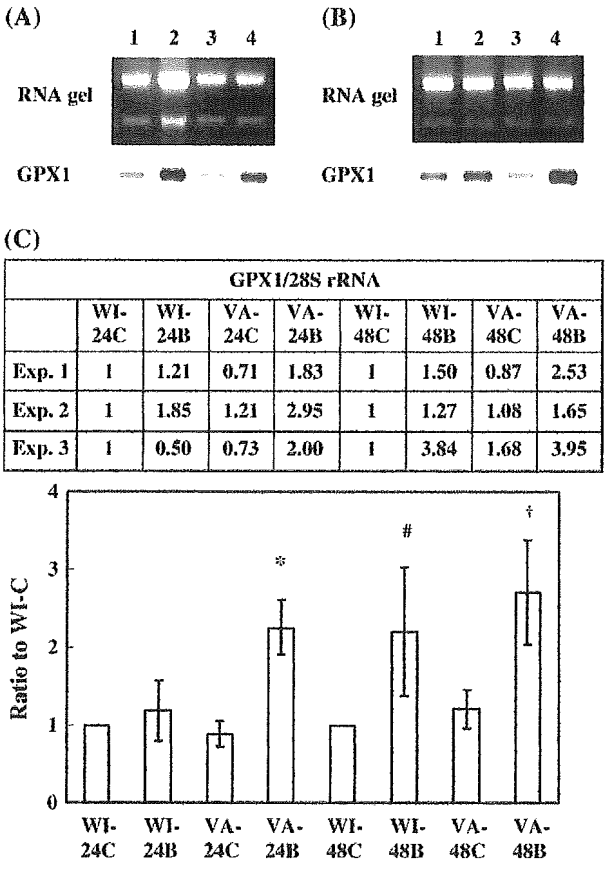


Fig. 5. Results of Northern blot analysis for the detection of GPX1 RNA levels following BLM treatment. (A) The RNA gel and transcript levels of GPX1 from cells treated for 24 h. (B) The RNA gel and transcript levels of GPX1 from cells treated for 48 h. (C) The density of GPX1 gene on the film was normalized by that of 28S rRNA bands on RNA gels. The relative changes to the control of WI38 cells for each time point from three sets of experiments are presented in the upper table. Data in mean ± SE values calculated from three independent experiments are then presented in the lower graph. Upper and lower bands of RNA gels in (A) and (B) indicate 28S rRNA and 18S rRNA, respectively. 1, WI-C; 2, WI-BLM, 3, VA-C; 4, VA-BLM; C, control; B, BLM; $^{*}P < 0.01$ vs VA-C or WI-BLM; $^{\#}P < 0.1$ vs WI-C; $^{\dagger}P < 0.05$ vs VA-C.

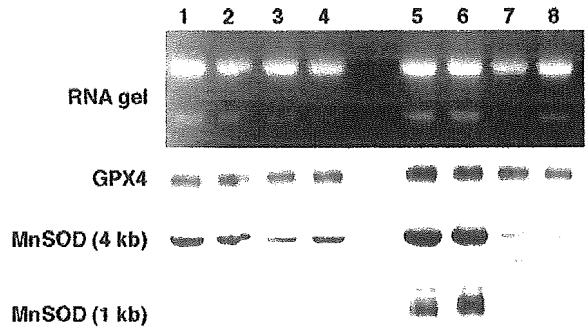


Fig. 6. Northern blot analysis for detecting RNA levels of GPX4 and MnSOD after 24-and 48-h BLM treatments. Groups 1 to 4 belong to the 24-h treatment groups. Groups 5 to 8 groups belong to the 48-h treatment groups. 1 and 5, WI-C; 2 and 6, WI-BLM; 3 and 7, VA-C; 4 and 8, VA-BLM.

indicated that NAC can react with hydrogen peroxide but its slow reaction with superoxide is not considered physiologically significant [52–54]. Moreover, unlike cisplatin [51], depletion of GSH as a target in BLM-induced cytotoxicity has not been indicated previously and it has been shown that reduction of ferric BLM complex to Fe(II)-BLM complex by glutathione or superoxide is important for forming activated BLM to damage DNA in vitro [2]. Chattopadhyay et al. showed that the clastogenic activity of BLM on normal lymphocytes was reduced after GSH depletion and enhanced after GSH addition [55]. Our results that NAC had no effect on cytotoxicity of both cells indicate that either GSH from NAC or NAC itself was not the appropriate antioxidant against BLM-induced oxidative stress or antioxidant effects of NAC outside the nucleus was compromised by the ROS-independent DNA damage promoted by GSH after BLM treatment. On the other hand, whether increased GSH or NAC in cytosol could also enhance their amount in mitochondria was also uncertain as a specific carrier is required for the transport of GSH into mitochondria [56] if mitochondrion is a source of oxidative stress in BLM-induced toxicity.

It has been hypothesized by Oberley that a lower MnSOD level is a characteristic of tumor cells [34] and reversion of transformed phenotypes by overexpression of MnSOD could be due to increased levels of hydrogen peroxide [57]. However, it has also been shown that elevated MnSOD levels in cultured tumor cells reduced oxidative stress in other studies without increased basal levels of hydrogen peroxide [41,50]. In the current study, we showed that markedly lower MnSOD and CAT activities in VA13 cells in fact were associated with higher DHR-detectable ROS levels. Lower MnSOD activities and higher GSH levels in VA13 cells [37] may actually promote formation of damaging glutathionyl radicals ($GS^{\cdot}$) in the mitochondria [53]. Moreover, antioxidant enzymes may play different roles in normal versus tumor cells via mechanisms independent of hydrogen peroxide. For example, overexpression of MnSOD in transgenic mice could protect hearts against toxicity induced by adriamycin [58,59], which generates superoxide, but reduced radiation control dose in fibrosarcoma cells when grown in mice [60]. On the other hand, it has been shown that human MnSOD has two major transcripts in the length of about 1 and 4 kb [61]. Our study not only confirmed lower MnSOD activities in VA13 cells that have been previously reported [36], but also first showed that both transcripts of MnSOD were higher in WI38 cells than in VA13 cells. Levels of 4-kb transcripts were much higher than that of 1-kb transcripts in both cells. Although whether the 4-kb transcript is functional has never been studied, it is very possible that the 4-kb transcript also contributes to the difference in MnSOD activities observed. In addition to lower MnSOD activities, we also found that activities of CAT were lower in VA13 cells, but activities of CuZnSOD and GPX were unchanged.

Our study is the first to demonstrate induction of GPX1 transcripts along with the increase of GPX activity by BLM. Previous studies studying BLM and antioxidant enzymes did not investigate transcript levels. Some studies detecting GPX mRNA levels also did not specify which form of GPX gene was detected [23,24]. It has been shown that the 5′-flanking region of the human GPX1 gene contains AP-1-binding sites and oxygen-responsive elements (ORE), which could contribute to the regulation of this gene by phorbol ester, oxygen tension, and xenobiotics [22,62,63]. It has also been found that the increase of nitric oxide level caused inactivation of GPX but induction of GPX gene expression [24] and ozone increased both activities and RNA levels of GPX in rat lungs [64]. Therefore, GPX is not necessarily only specifically induced by hydrogen peroxide but can respond to altered redox status modulated by different conditions. Results from this study suggest that GPX1 gene induction was responsible for increased GPX activities following BLM treatment in both cells. However, the increase of GPX activities in WI38 cells occurred later than the increase of ROS levels and GPX1 induction preceded ROS increase in VA13 cells, indicating differential regulation of GPX1 by BLM in these two cells. The differential responses of GPX1 in WI38 and VA13 cells to BLM could be due to altered redox regulation of gene expression or signal transduction following transformation. It is possible that molecules other than DHR-detectable ROS but related to oxidative stress following BLM treatment induced GPX1. Alternatively, GPX1 in VA13 cells was more easily induced by smaller increase of ROS that became insignificant compared to higher basal levels of ROS in VA13 cells. Furthermore, since the majority of GPX1 should be present in the cytosol, increased GPX1 may not compensate for oxidative stress in mitochondria completely. On the other hand, we did not observe any change in the activities of MnSOD, CuZnSOD, and CAT following BLM treatment. It has been shown that those antioxidant enzymes responded to the same sources of ROS in a different manner. For example, Shull et al. showed that hydrogen peroxide treatment resulted in more GPX and CAT transcript levels but not CuZnSOD levels in the tracheal epithelial cell line, while superoxide generated extracellularly from the xanthione/xanthione oxidase system induced only MnSOD mRNA levels but not that of GPX, CAT, and CuZnSOD [23]. Since other primary antioxidant enzymes were not altered by BLM treatment in our study, why GPX1 was selectively induced and its role in BLM-induced cytotoxicity or possibly BLM resistance remain to be investigated.

In conclusion, our results indicate that BLM caused oxidative stress at an earlier time point in WI38 cells, although it induced higher cytotoxicity in VA13 cells. The use of normal or tumor cells in studying oxidative stress and toxicity induced by BLM may therefore have distinct implications. In addition to differential responses between WI38 and VA13 cells to BLM, the role of selective GPX1 induction by BLM also has implications in understanding

chemotherapy using BLM and cellular or molecular events not directly related to the interaction of BLM with nuclear DNA.

## Acknowledgments

This work was supported by Grants NSC 89-2314-B-182-070 and NSC 90-2320-B-182-061 from National Science Council, Taiwan. We thank Dr. Daret K. St. Clair at the University of Kentucky for helpful discussion.

## References

[1] Hay, J.; Shahzeidi, S.; Laurent, G. Mechanisms of bleomycin-induced lung damage. *Arch. Toxicol.* **65:**81–94; 1991.

[2] Sugiura, Y.; Suzuki, T.; Kuwahara, J.; Tanaka, H. On the mechanism of hydrogen peroxide-, superoxide-, and ultraviolet light-induced DNA cleavages of inactive bleomycin-iron (III) complex. *Biochem. Biophys. Res. Commun.* **105:**1151–1158; 1982.

[3] Oberley, L. W.; Buettner, G. R. The production of hydroxyl radical by bleomycin and iron (II). *FEBS Lett.* **97:**47–49; 1979.

[4] Buettner, G. R.; Moseley, P. L. Ascorbate both activates and inactivates bleomycin by free radical generation. *Biochemistry* **21:**9784–9978; 1992.

[5] Mahmutoglu, I.; Scheulen, M. E.; Kappus, H. Oxygen radical formation and DNA damage due to enzymatic reduction of bleomycin-Fe(III). *Arch. Toxicol.* **60:**150–153; 1987.

[6] Kanofsky, J. R. Singlet oxygen production by bleomycin. *J. Biol. Chem.* **261:**13546–13550; 1986.

[7] Gutteridge, J. M. C.; West, M.; Eneff, K.; Floyd, R. A. Bleomycin-iron damage to DNA with formation of 8-hydroxydeoxyguanosine and base propenals. Indication that xanthine oxidase generates superoxide from DNA degradation products. *Free Radic. Res. Commun.* **10:**159–165; 1990.

[8] Turner, M. J.; Bozarth, C. H.; Strauss, K. E. Evidence for intracellular superoxide formation following the exposure of guinea pig erythrocytes to bleomycin. *Biochem. Pharmacol.* **38:**85–90; 1999.

[9] Benitez-Bribiesca, L.; Sanchez-Suarez, P. Oxidative damage, bleomycin, and gamma radiation induce different types of DNA strand breaks in normal lymphocytes and thymocytes. *Ann. N.Y. Acad. Sci.* **887:**133–149; 1999.

[10] Giri, S. N.; Chen, Z. L.; Younker, W. R.; Schiedt, M. J. Effects of intratracheal administration of bleomycin on GSH-shuttle enzymes, catalase, lipid peroxidation, and collagen content in the lungs of hamster. *Toxicol. Appl. Pharmacol.* **71:**132–141; 1983.

[11] Khadir, A.; Verreault, J.; Averill, D. A. Inhibition of antioxidants and hyperthermia enhance bleomycin-induced cytotoxicity and lipid peroxidation in Chinese hamster ovary cells. *Arch. Biochem. Biophys.* **370:**163–175; 1999.

[12] Roberts, L. J. II; Morrow, J. D. Measurement of F2-isoprostanes as an index of oxidative stress in vivo. *Free Radic. Biol. Med.* **28:**505–513; 2000.

[13] Gajewski, E.; Aruoma, O. I.; Dizdaroglu, M.; Halliwell, B. Bleomycin-dependent damage to the bases in DNA is a minor side reaction. *Biochemistry* **30:**2444–2448; 1991.

[14] Halliwell, B.; Gutteridge, J. M. C. *Free radicals in biology and medicine*. New York: Oxford University Press; 1999.

[15] Zelko, I. N.; Mariani, T. J.; Folz, R. J. Superoxide dismutase multigene family: a comparison of the CuZn-SOD (SOD1), Mn-SOD (SOD2), and EC-SOD (SOD3) gene structures, evolution, and expression. *Free Radic. Biol. Med.* **33:**337–349; 2002.

[16] Imai, H.; Nakagawa, Y. Biological significance of phospholipid hydroperoxide glutathione peroxidase (PHGPx, GPx4) in mammalian cells. *Free Radic. Biol. Med.* **34:**145–169; 2003.

[17] Esposito, L. A.; Kokoszka, J. E.; Waymire, K. G.; Cottrell, B.; MacGregor, G. R.; Wallace, D. C. Mitochondrial oxidative stress in mice lacking the glutathione peroxidase-1 gene. *Free Radic. Biol. Med.* **28:**754–766; 2000.

[18] Akashi, M.; Hachiya, M.; Paquette, R. L.; Osawa, Y.; Shimizu, S.; Suzuki, G. Irradiation increases manganese superoxide dismutase mRNA levels in human fibroblasts. *J. Biol. Chem.* **270:** 15864–15869; 1995.

[19] Wong, G. H. W.; Goeddel, D. V. Induction of manganous superoxide dismutase by tumor necrosis factor: possible protective mechanism. *Science* **241:**941–944; 1988.

[20] Crosby, A.; Wahle, K. W. J.; Duthie, G. G. Modulation of glutathione peroxidase activity in human vascular endothelial cells by fatty acids and the cytokine interleukin-1β. *Biochim. Biophys. Acta* **1303:**187–192; 1996.

[21] Quinlan, T.; Spivack, S.; Mossman, B. T. Regulation of antioxidant enzymes in lung after oxidant injury. *Environ. Health Perspect.* **102 (Suppl. 2):**79–87; 1994.

[22] Jornot, L.; Junod, A. F. Hyperoxia, unlike phorbol ester, induces glutathione peroxidase through a protein kinase C-independent mechanism. *Biochem. J.* **326:**117–123; 1997.

[23] Shull, S.; Heintz, N. H.; Periasamy, M.; Manohar, M.; Janssen, Y. M. W.; Marsh, J. P.; Mossman, B. T. Differential regulation of antioxidant enzymes in response to oxidants. *J. Biol. Chem.* **266:**24398–24403; 1991.

[24] Dobashi, K.; Asayama, K.; Nakane, T.; Kodera, K.; Hayashibe, H.; Nakazawa, S. Induction of glutathione peroxidase in response to inactivation by nitric oxide. *Free Radic. Res.* **35:**319–327; 2001.

[25] Dalton, T. P.; Puga, A. Regulation of gene expression by reactive oxygen. *Annu. Rev. Pharmacol. Toxicol.* **39:**67–101; 1999.

[26] Xu, Y.; Kiningham, K. K.; Devalaraja, M. N.; Yeh, C. C.; Majima, H.; Kasarskis, E. J.; St.Clair, D. K. An intronic NF-kappaB element is essential for induction of the human manganese superoxide dismutase gene by tumor necrosis factor-α and interleukin-1β. *DNA Cell Biol.* **18:**709–722; 1999.

[27] Phan, S. H.; Fantone, J. C. Inhibition of bleomycin-induced pulmonary fibrosis by lipopolysaccharide. *Lab. Invest.* **50:**587–591; 1984.

[28] Filderman, A. E.; Genovese, L. A.; Lazo, J. S. Alterations in pulmonary protective enzymes following systemic bleomycin treatment in mice. *Biochem. Pharmacol.* **37:**1111–1116; 1988.

[29] Fantone, J. C.; Phan, S. H. Oxygen metabolite detoxifying enzyme levels in bleomycin-induced fibrotic lungs. *Free Radic. Biol. Med.* **4:**388–402; 1988.

[30] Hiraiwa, K.; Oka, T.; Yagi, K. Effect of bleomycin on lipid peroxides, glutathione peroxidase and collagenase in cultured lung fibroblasts. *J. Biochem.* **93:**1203–1210; 1983.

[31] Allen, R. G.; Balin, A. K. Effects of oxygen on the antioxidant responses of normal and transformed cells. *Exp. Cell Res.* **289:** 307–316; 2003.

[32] Hileman, E. O.; Liu, J.; Albitar, M.; Keating, M. J.; Huang, P. Intrinsic oxidative stress in cancer cells: a biochemical basis for therapeutic selectivity. *Cancer Chemother. Pharmacol.* **53:**209–219; 2004.

[33] Bize, I. B.; Oberley, L. W.; Morris, H. P. Superoxide dismutase and superoxide radical in Morri Hepatomas. *Cancer Res.* **40:**3369–3686; 1980.

[34] Oberley, L. W.; Oberley, T. D. Role of antioxidant enzymes in cell immortalization and transformation. *Mol. Cell. Biol.* **84:**147–153; 1988.

[35] Yen, H.-C.; Nien, C.-Y.; Majima, H.J.; Lee, C.-P.; Chen, S.-Y.; Wei, J.-S.; See, L.-C. Increase of lipid peroxidation by cisplatin in WI38 cells but not in SV40-transformed WI38 cells. *J. Biochem. Mol. Toxicol.* **17:**39–46; 2003.

[36] Oberley, L. W.; McCormick, M. L.; Sierra-Rivera, E.; St.Clair, D. K. Manganese superoxide dismutase in normal and transformed human embryonic lung fibroblasts. *Free Radic. Biol. Med.* **6:**379–384; 1989.

[37] Wan, X. S.; St.Clair, D. K. Differential cytotoxicity of buthionine sulfoximine to "normal" and transformed human lung fibroblast cells. *Cancer Chemother. Pharmacol.* **33:**210–214; 1993.

[38] Chabot, B.; Frappier, D.; Branche, H. L. Differential ASF/SF2 activity in extracts from normal WI38 and transformed WI38VA13 cells. *Nucleic Acids Res.* **20:**5197–5204; 1992.

[39] Chen, Z. P.; Schell, J. B.; Ho, C.-T.; Chen, K. Y. Green tea epigallocatechin gallate shows a pronounce growth inhibitory effect on cancerous cells but not on their normal counterparts. *Cancer Lett.* **129:**173–179; 1998.

[40] Haugland, R. P. *Handbook of fluorescent probes and research products*. Web edition. Eugene: Molecular Probes; 2002.

[41] Motoori, S.; Majima, H. J.; Ebara, M.; Kato, H.; Hirai, F.; Kakinuma, S.; Yamaguchi, C.; Ozawa, T.; Nagano, T.; Tsujii, H.; Saisho, H. Overexpression of mitochondrial manganese superoxide dismutase protects against radiation-induced cell death in the human hepatocellular carcinoma cell line HLE. *Cancer Res.* **61:**5382–5388; 2001.

[42] Hirai, F.; Motoori, S.; Kakinuma, S.; Tomita, K.; Indo, H. P.; Yamaguchi, T.; Yen, H.-C.; St.Clair, D. K.; Nagano, T.; Ozawa, T.; Saisho, H.; Majima, H. J. Mitochondrial signal lacking manganese superoxide dismutase failed to prevent cell death by reoxygenation following hypoxia in a human pancreatic cancer cell line, KP4. *Antioxid. Redox Sign.* **6:**523–535; 2004.

[43] Spitz, D. R.; Oberley, L. W. An assay for superoxide dismutase activity in mammalian tissue homogenates. *Anal. Biochem.* **179:**8–18; 1989.

[44] Beers, R. F.; Sizer, I. W. A spectrophotometric method for measuring the breakdown of hydrogen peroxide by catalase. *J. Biol. Chem.* **195:**133–140; 1952.

[45] St. Clair, D. K.; Chow, C. K. Glutathione peroxidase: activity and steady-state level of mRNA. In: Punchard, N. A., Kelly, F. J., eds. *Free radicals. A practical approach*. New York: Oxford University Press; 1996: pp. 227–240.

[46] Yen, H.-C.; Chen, B.-S.; Hsu, Y.-T. Effect of anticoagulants and storage of coupling reagent on the activity assay of extracellular glutathione peroxidase in human plasma. *J. Biomed. Lab. Sci.* **16:**6–10; 2004.

[47] Pfanner, N.; Wiedemann, N. Mitochondrial protein import: two membranes, three translocases. *Curr. Opin. Cell Biol.* **14:**400–411; 2002.

[48] Royall, J. M.; Ischiropoulos, H. Evaluation of 2′-7′-dichlorofluorescin and dihydrorhodamine 123 as fluorescent probes for intracellular $H_2O_2$ in cultured endothelial cells. *Arch. Biochem. Biophys.* **302:**348–355; 1993.

[49] Kooy, N. W.; Royall, J. M.; Ischiropoulos, H.; Beckman, J. S. Peroxynitrite-mediated oxidation of dihydrorhodamine 123. *Free Radic. Biol. Med.* **16:**149–156; 1994.

[50] Majima, H. J.; Oberley, T. D.; Furukawa, K.; Mattson, M. P.; Yen, H.-C.; Szweda, L. I.; St.Clair, D. K. Prevention of mitochondrial injury by manganese superoxide dismutase reveals a primary mechanism for alkaline-induced cell death. *J. Biol. Chem.* **273:**8217–8224; 1998.

[51] Salahudeen, A.; Poovala, V.; Parry, W.; Pande, R.; Kanji, V.; Ansari, N.; Morrow, J.; Roberts, J., II. Cisplatin induces N-acetyl cysteine suppressible $F_2$-isoprostane production and injury in renal tubular epithelial cells. *J. Am. Soc. Nephrol.* **9:**1445–1448; 1998.

[52] Winterbourn, C. C.; Metodiwa, D. Reactivity of biologically important thiol compounds with superoxide and hydrogen peroxide. *Free Radic. Biol. Med.* **27:**322–328; 1999.

[53] Jones, C. M.; Lawrence, A.; Wardman, P.; Burkitt, M. J. Kinetics of superoxide scavenging by glutathione: an evaluation of its role in the removal of mitochondrial superoxide. *Biochem. Soc. Trans.* **31:** 1337–1339; 2003.

[54] Aruoma, O. I.; Halliwell, B.; Hoey, B. M.; Butler, J. The antioxidant action of N-acetylcysteine: its reaction with hydrogen peroxide, hydroxyl radical, superoxide, and hypochlorus acid. *Free Radic. Biol. Med.* **6:**593–597; 1989.

[55] Chattopadhyay, A.; Choudhury, S.; Chatterjee, A. Modulation of clastogenic activity of bleomycin by reduced-glutathione, glutathione-ester and buthionine sulfoximine. *Mutagenesis* **12:**221–225; 1997.

[56] Fernandez-Checa, J. C.; Kaplowitz, N.; Garcia-Ruiz, C.; Colell, A.; Miranda, M.; Mari, M.; Ardite, E.; Morales, A. GSH transport in mitochondria: defense against TNF-induced oxidative stress and alcohol-induced defect. *Am. J. Physiol.* **273:**G7–G17; 1997.

[57] Zhong, W.; Oberley, L. W.; Oberley, T. D.; Yan, T.; Domann, F. E.; St.Clair, D. K. Inhibition of cell growth and sensitization to oxidative damage by overexpression of manganese superoxide dismutase in rat glioma cells. *Cell Growth Differ.* **7:**1175–1186; 1996.

[58] Yen, H.-C.; Oberley, T. D.; Vichitbandha, S.; Ho, Y.-S.; St.Clair, D. K. The protective role of manganese superoxide dismutase against adriamycin-induced acute cardiac toxicity in transgenic mice. *J. Clin. Invest.* **98:**1253–1260; 1996.

[59] Yen, H.-C.; Oberley, T. D.; Gairola, C. G.; Szweda, L. I.; St.Clair, D. K. Manganese superoxide dismutase protects mitochondrial complex I against adriamycin-induced cardiomyopathy in transgenic mice. *Arch. Biochem. Biophys.* **362:**59–66; 1999.

[60] Urano, M.; Kuroda, M.; Reynolds, R.; Oberley, T. D.; St.Clair, D. K. Expression of manganese superoxide dismutase reduced tumor control radiation dose: gene-radiotherapy. *Cancer Res.* **55:**2490–2493; 1995.

[61] Wispe, J. R.; Clark, J. C.; Burhans, M. S.; Kropp, K. E.; Korfhagen, T. R.; Whitsett, J. A. Synthesis and processing of the precursor for human mangano-superoxide dismutase. *Biochim. Biophys. Acta* **994:**30–36; 1989.

[62] Cowan, D. B.; Weisel, R. D.; Williams, W. G.; Mickle, D. A. G. Identification of oxygen responsive elements in the 5-flanking region of the human glutathione peroxidase gene. *J. Biol. Chem.* **268:** 26904–26910; 1993.

[63] Moscow, J. A.; Morrow, C. S.; He, R.; Mullenbach, G. T.; Cowan, K. H. Structure and function of the 5-flanking sequence of the human cytosolic selenium-dependent glutathione peroxidase gene (hgpx1). *J. Biol. Chem.* **267:**5949–5958; 1992.

[64] Rahman, I.; Clearch, L. B.; Massaro, D. Rat lung antioxidant enzyme induction by ozone. *Am. J. Physiol.* **260:**L412–L418; 1991.

# Increased expression of humanin peptide in diffuse-type pigmented villonodular synovitis: implication of its mitochondrial abnormality

K Ijiri, H Tsuruga, H Sakakima, K Tomita, N Taniguchi, K Shimoonoda, S Komiya, M B Goldring, H J Majima and T Matsuyama

*Ann. Rheum. Dis* 2005;64;816-823; originally published online 26 Nov 2004; doi:10.1136/ard.2004.025445

EXTENDED REPORT

# Increased expression of humanin peptide in diffuse-type pigmented villonodular synovitis: implication of its mitochondrial abnormality

K Ijiri, H Tsuruga, H Sakakima, K Tomita, N Taniguchi, K Shimoonoda, S Komiya, M B Goldring, H J Majima, T Matsuyama

*Ann Rheum Dis* 2005;64:816–823. doi: 10.1136/ard.2004.025445

See end of article for authors' affiliations

Correspondence to: Dr K Ijiri, Beth Israel Deaconess Medical Center, Harvard Institutes of Medicine, Room 237, 4 Blackfan, Circle, Boston, MA 02115, USA; kijiri@bidmc.harvard.edu

Accepted 27 October 2004
**Published Online First 26 November 2004**

**Objectives:** To define the pathogenesis of pigmented villonodular synovitis (PVNS), by searching for highly expressed genes in primary synovial cells from patients with PVNS.
**Methods:** A combination of subtraction cloning and Southern colony hybridisation was used to detect highly expressed genes in PVNS in comparison with rheumatoid synovial cells. Northern hybridisation was performed to confirm the differential expression of the humanin gene in PVNS. Expression of the humanin peptide was analysed by western blotting and immunohistochemistry. Electron microscopic immunohistochemistry was performed to investigate the distribution of this peptide within the cell.
**Results:** 68 highly expressed genes were identified in PVNS. Humanin genes were strongly expressed in diffuse-type PVNS, but were barely detected in nodular-type PVNS, rheumatoid arthritis, or osteoarthritis. Humanin peptide was identified in synovium from diffuse-type PVNS, and most of the positive cells were distributed in the deep layer of the synovial tissue. Double staining with anti-humanin and anti-heat shock protein 60 showed that humanin was expressed mainly in mitochondria. Electron microscopy disclosed immunolocalisation of this peptide, predominantly around dense iron deposits within the siderosome.
**Conclusions:** Increased expression of the humanin peptide in mitochondria and siderosomes is characteristic of synovial cells from diffuse-type PVNS. Humanin is an anti-apoptotic peptide which is encoded in the mitochondrial genome. Present findings suggest that mitochondrial dysfunction may be the principal factor in pathogenesis of diffuse-type PVNS and that humanin peptide may play a part in the neoplastic process in this form of PVNS.

Pigmented villonodular synovitis (PVNS) is classified as an uncommon idiopathic proliferative synovial process.[1 2] It can exist in a localised form within a joint but more commonly occurs as a diffuse form where the entire synovium of a joint is affected.[3–7] The exact aetiology of PVNS is still unknown.[8–10] Previous experimental and epidemiological studies have suggested that PVNS is a reactive process involving a chronic inflammatory response.[11 12] However, recent studies showing the capacity of these lesions for autonomous growth and the potential for recurrence have suggested involvement of a neoplastic process.[13] The neoplastic hypothesis has been further supported by studies suggesting that heterogeneous proliferating cells, such as fibroblasts, histiocytes, multinuclear cells, and chronic inflammatory cells, might be neoplastic, with other cell types being reactive in nature.[14 15]

Histologically, PVNS is composed of proliferating mononuclear cells, with frequent giant cells, and intracellular and extracellular iron deposits. These iron deposits are observed as membrane bound particles in siderosomes. Interestingly, Schumacher *et al* and Ghadially *et al* reported that the siderosome fuses with mitochondria in deep synovial cells from patients with PVNS.[16 17] Moreover, abundant mitochondria throughout the cytoplasm were observed in dispersed stromal cells containing electron dense inclusions and in giant cells.[16 18]

In this study we searched for highly expressed genes in primary synovial cells from patients with PVNS compared with those from patients with rheumatoid arthritis (RA). We considered that a comparison of synovial cells from PVNS with those from RA, which are composed of chronic inflammatory cells, would identify the distinct nature of PVNS and define this proliferative process more precisely. Ribosomal RNA (rRNA) with poly A tail encoded by mitochondrial genes was highly expressed in PVNS. Among these genes, humanin has been reported to act as an oncopeptide or as an anti-apoptotic factor against Bax (Bcl2 associated X protein), which is an apoptosis-inducing protein.[19 20] However, little is known about the pathological role of humanin in diseases other than Alzheimer's disease.

We report here that the expression of humanin peptide is increased strongly in diffuse-type PVNS compared with other arthritides and it is abundant in mitochondria and siderosomes of synovial cells from PVNS.

## METHODS

### Synovial tissue preparation and RNA extraction

Synovial biopsy specimens were obtained during surgery from six patients with PVNS, three with RA, and three with osteoarthritis (OA). These lesions were subtyped into two types (diffuse or nodular) according to locations (intra-articular versus extra-articular) and pathological growth patterns, which reflected clinical characteristics and biological behaviour.[13]

**Abbreviations:** BSA, bovine serum albumin; GAPDH, glyceraldehyde-3-phosphate dehydrogenase; hsp, heat shock protein; IMDM, Iscove modified Dulbecco's medium; OA, osteoarthritis; PBS, phosphate buffered saline; PCR, polymerase chain reaction; PVNS, pigmented villonodular synovitis; RA, rheumatoid arthritis; RT-PCR, reverse transcriptase-polymerase chain reaction; SDS, sodium dodecyl sulphate; SDS-PAGE, sodium dodecyl sulphate-polyacrylamide gel electrophoresis; SSC, saline sodium citrate

The patients with RA met the criteria of the 1987 American College of Rheumatology. The tissue was cultured in Iscove modified Dulbecco's medium (IMDM) with collagenase V (1 mg/ml medium) for 40 minutes and cells were harvested through mesh and gathered by centrifugation. Total cellular RNA was extracted using acid-guanidinium-phenol-chloroform (AGPC) methods.[21] Equal aliquots were then electrophoresed on 1% agarose gels stained with ethidium bromide to compare large and small rRNA qualitatively and to exclude degradation. Poly $A^+$ RNA was purified from total RNA using the First Track kit (Invitrogen).

### Double stranded cDNA synthesis and subtraction cloning

One microgram of total RNA sample was used to synthesise full length, double stranded cDNA using a SMART polymerase chain reaction (PCR) cDNA synthesis kit (Clontech). Subtraction cloning was performed with a PCR-Select cDNA subtraction kit (Clontech). Equal amounts of double stranded cDNAs from two patients with PVNS (diffuse type/lane 1, nodular type/lane 2 in fig 2) were used as tester cDNAs, and equal amounts of double stranded cDNAs from three patients with RA were used as driver cDNAs. PCR using CD163 primers was performed to estimate the efficiency of subtraction, and the expected decrease in CD163 in the subtracted sample was observed (data not shown).

### Southern colony hybridisation

Subtracted cDNAs were ligated to TOPO vector (Invitrogen) and transformed into DH10B cells (Invitrogen) by electroporation. After blue-white selection with X-gal containing Luria-Bertani (LB) plates, white colonies were cultured overnight with 150 µl LB medium in sterile 1.5 ml tubes and centrifuged for 2 minutes at 12 000 g, and the pellet was resuspended in 10 µl LB medium. The medium was mixed completely and 2 µl was dotted onto a nylon membrane for Southern hybridisation. SMART double stranded cDNA was labelled with [$^{32}$P]dCTP by random priming (Stratagene). Membranes were hybridised in aqueous solution (5 × saline sodium citrate (SSC), Denhardt's solution, 0.1% sodium dodecyl sulphate (SDS), 10 mg salmon sperm DNA) overnight at 65°C. After washing at 65°C for 1 hour in 0.1 × SSC, 0.1% SDS, the membranes were exposed to *x* ray film (Eastman Kodak Co) with an intensifying screen at −80°C. Measurement of cDNA was performed by scanning with a BASS 1000 Densitometer (Fuji film), and normalisation against glyceraldehyde-3-phosphate dehydrogenase (GAPDH) cDNA hybridised subsequently on the same blots.

**Table 1** Highly expressed genes in PVNS compared with RA

| Genes | No |
|---|---|
| *Mitochondrial* | |
| 16S rRNA | 30 |
| 12S rRNA | 5 |
| Homosapiens tomoregulin mRNA | 2 |
| Homosapiens ARFGAP 1 protein mRNA | 1 |
| Mitochondrial proteolipid 68 MP homology | 1 |
| *Inflammation* | |
| $\beta_2$-Microglobulin mRNA | 4 |
| Transforming growth factor-β mRNA | 1 |
| *Fibrogenolysis* | |
| Arg/serpin 1 plasminogen activator-inhibitor 2 mRNA | 1 |
| Homosapiens similar to serine proteinase mRNA | 1 |
| Homosapiens similar to serine/arginine repetitive matrix mRNA | 1 |
| *Iron metabolism* | |
| Ferritin light chain mRNA | 13 |
| *Cartilage degradation* | |
| Homosapiens dihydropyrimidinase mRNA | 1 |
| Homosapiens osteopontin mRNA | 1 |
| *Neoplastic* | |
| L-Plastin mRNA | 1 |
| *Others* | |
| Eukaryotic translation elongation factor mRNA | 2 |
| Homosapiens Nef-associated factor mRNA | 1 |
| Unknown | 2 |
| Total | 68 clones |

### DNA sequencing

Sixty eight cDNAs from differentially expressed clones were amplified with M13 reverse (5'-CAGGAAACAGCTATGAC-3') primers using thermal cycling conditions (96°C for 30 seconds, 50°C for 15 seconds, 60°C for 4 minutes for 25 cycles). The cDNAs were purified and sequenced using the ABI PRISM dye terminator cycle sequencing ready reaction kit with template suppression reagent (ABI PRISM). DNA sequences were analysed using DNASIS software and compared with sequences in GeneBank (National Center for Biotechnology Information, Bethesda, MD).

### Northern hybridisation

Poly $A^+$ RNA (168 ng) samples of the synovium from five patients with PVNS, three with RA, and three with OA patients were loaded and fractionated through 1.0% agarose gels and transferred to Hybond-N+ nylon transfer membrane (Amersham). Purified human cDNA (40 ng) was labelled with [$^{32}$P]dCTP by random priming and applied to the membrane for hybridisation in aqueous solution (5 × SCC, Denhardt's solution, 0.1% SDS, 10 mg salmon sperm DNA, 50% formamide) overnight at 42°C. After washing at 42°C for 1 hour in 0.1 x SSC, 0.1% SDS, the membranes were exposed to *x* ray film (Eastman Kodak Co) with an intensifying screen at −80°C.

### Semiquantitative reverse transcriptase-polymerase chain reaction (RT-PCR)

Total RNA (2.5 µg) from five patients with PVNS, three with RA, and two with OA was used for cDNA synthesis with oligo$(dT)_{12-18}$ as template primer using M-MuLV reverse transcriptase. The reaction was conducted in a final volume of 50 µl containing 1 ml of the transcribed cDNA probe, 200 µmol/l of each dNTP, 1 × PCR buffer including 1.5 mM $MgCl_2$ (Takara Biomedical), 0.4 µM forward and reverse primers, and 2.5 U Taq polymerase (Takara). All amplimers were amplified simultaneously with GAPDH as internal standard. The respective primer pairs were for cytochrome *c* (forward: 5'-GCATAAACAACATAAGCTTCTGA-3', reverse: 5'-CAGCAGATCATTTCATATTGCTT-3'), for ATPase (forward: 5'-TCTCATCAACAACCGACTAATCA-3', reverse: 5'-GATAAGTGTAGAGGGAAGGTTAA-3'), for NADH dehydrogenase (forward: 5'-TTTACTCAATCCTCTGATCAGGG-3', reverse: 5'-CGAATTCATAAGAACAGGGAGGT-3'), and for cytochrome *b* (forward: 5'-AATTACAAACTTACTATCCGCCA-3', reverse: 5'-TGGGCGAAATATTATGCTTTGTT-3'). The reaction mixtures were incubated for 3 minutes at 94°C, followed by 32 cycles of denaturation for 1 minute at 94°C, annealing for 1.5 minutes at 52°C, and extension for 1 minute at 72°C.

### Cell and tissue processing for light microscopy and immunohistochemistry

To isolate synovial cells, the deep layers of synovium from diffuse-type PVNS were cultured in IMDM with collagenase

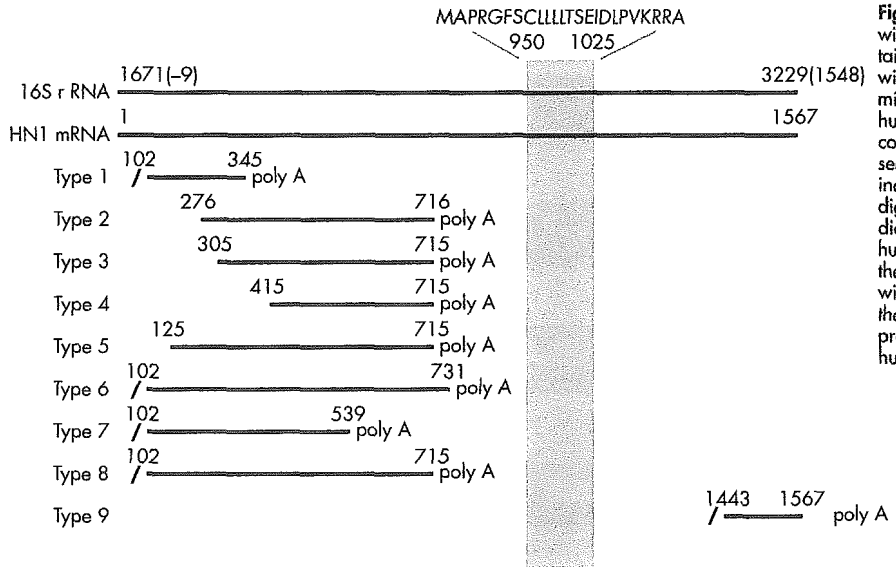


**Figure 1** The sequences encoded within the 16S rRNA region with poly A tail. The cDNA fragments were aligned with the 16S rRNA region of the mitochondrial gene and the correlating humanin mRNA sequence. Southern colony hybridisations repeated these sequences in a total of three rounds independently. Oblique bars show the digestion sites by Rsa I and upward diagonal bar shows the region of humanin coding sequences. Although there are nine types of sequences with poly A tail within this region, only the type 9 sequence was identical to the previously reported mRNA encoding humanin peptide.

V (1 mg/ml medium) for 20 minutes and cells were harvested through mesh and gathered by centrifugation. These synovial cells were cultured in IMDM with 10% fetal bovine saline for 4 hours and fixed with 10% buffered formaldehyde at room temperature for 10 minutes, then rinsed with phosphate buffered saline (PBS). Formalin fixed tissue sections were also used for immunostaining. A rabbit polyclonal anti-humanin antibody was synthesised and purified on an affinity column and dissolved in PBS (0.9% NaCl, 0.02 M phosphate buffer, pH 7.0). The IgG concentration was analysed using a protein assay kit (Bio-Rad). Immunostaining was performed as previously described.[22 23] Briefly, cells and sections were fixed with 4% formaldehyde in PBS. After rinsing with PBS, membrane perforation treatment was performed with 95% ethanol/5% acetic acid for 10 minutes. After washing with PBS and blocking by incubation with 1% bovine serum albumin (BSA), excess BSA was then removed and the cells were incubated with anti-humanin antibodies overnight at 4°C. After rinsing, Alexa Fluor 488 goat antirabbit IgG (Molecular Probes Inc) was applied as a secondary antibody for 60 minutes. Immunofluorescence was detected with a CSU-10 confocal laser scanning unit (Yokogawa Electric Co), coupled to an IX90 inverted microscope with UPlanAPOX20 objective lens (Olympus Potical Co), and C5810-01 colour chilled 3CCD camera (Hamamatsu Photonics, KK). For double staining, anti-humanin antibody and anti-heat shock protein (hsp) 60 antibody (Santa Cruz Biochemistry Inc) were used as first antibodies, while Alexa Fluor 568 goat antirabbit IgG and Alexa Fluor 488 donkey antigoat IgG (Molecular Probes Inc) were used as a second antibodies.

## Western blot analysis

Tissues were homogenised and lysed in a buffer consisting of 150 mM NaCl, 50 mM Tris HCl, pH 7.5, 0.5% Nonidet 40, 50 mM NaF, 1 mM $Na_3VO_4$, 1 mM phenylmethylsulphonyl fluoride, and 1% aprotinin at 4°C for 30 minutes. Cell lysates were cleared of cell debris by centrifugation at 14 000 *g* for 30 minutes. Protein (20 µg) was subjected to sodium dodecyl sulphate-polyacrylamide gel electrophoresis (SDS-PAGE) on

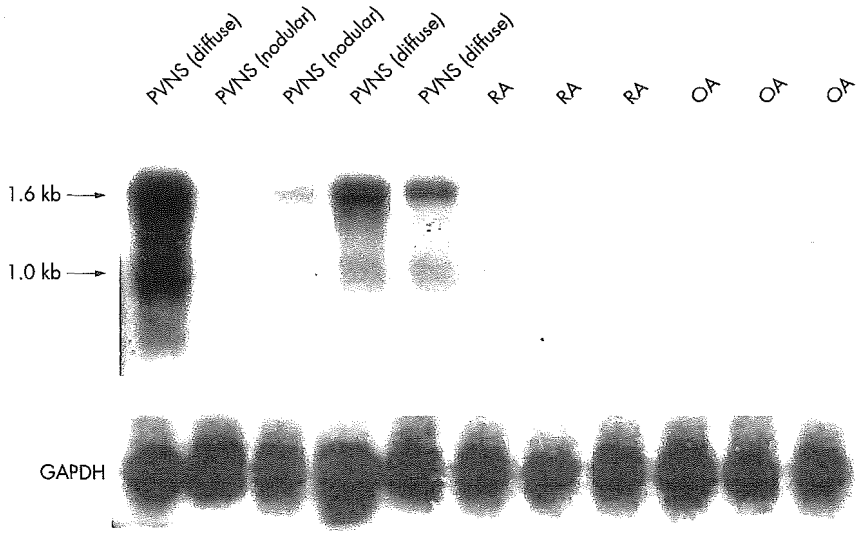


**Figure 2** Northern blot analysis of mRNAs expressed by synovial cells from patients with PVNS, RA, and OA. Total RNA (168 ng) was subjected to electrophoresis in a 1.0% agarose gel containing formaldehyde, transferred to a nylon membrane, and probed with [$^{32}$P]dCTP labelled cDNA (type 9; fig 1). Another cDNA (type 3) encoded in the 16S rRNA region was also used in northern blotting and the expression level and size were same as those using type 9 cDNA (data not shown). Humanin genes were strongly expressed in diffuse-type PVNS, but barely detected in nodular-type PVNS, RA, or OA. The size of the expressed major message was ~1.6 kb and the other messages were ~1 kb, which corresponds to the results of a previous report by Hashimoto *et al*.[28]